Revisiting Taylor's hypothesis in homogeneous turbulent shear flow

Frank Jacobitz, Kai Schneider

Revisiting Taylor's hypothesis in homogeneous turbulent shear flow

Frank G. Jacobitz [1,*] and Kai Schneider [2,†]

[1] *Mechanical Engineering Department, Shiley-Marcos School of Engineering, University of San Diego, 5998 Alcalá Park, San Diego, California 92110, USA*

[2] *Aix-Marseille Université, CNRS, Institut de Mathématiques de Marseille, 3 place Victor Hugo, 13331 Marseille cedex 3, France*

(Received 28 September 2023; accepted 14 March 2024; published 3 April 2024)

Taylor's hypothesis of frozen flow is revisited in homogeneous turbulent shear flow by examining the cancellation properties of Eulerian and convective accelerations at different flow scales. Using results of direct numerical simulations, vector-valued flow quantities, including the Lagrangian, Eulerian, and convective accelerations, are decomposed into an orthogonal wavelet series and their alignment properties are quantified through the introduction of scale-dependent geometrical statistics. Joint-probability density functions of the Eulerian and convective accelerations show antialignment at small scales of the turbulent motion, but this observation does not hold at large scales. Similarly, the angles of the scale-wise contributions of the Eulerian and convective accelerations were found to prefer an antiparallel orientation at small scales. Such antialignment, however, is not observed at the largest scales of the turbulent motion. The results suggest that Taylor's hypothesis holds at small scales of homogeneous turbulent shear flow, but not for large-scale motion. The Corrsin scale is proposed as a measure for the applicability of Taylor's hypothesis in such flows.

DOI: 10.1103/PhysRevFluids.9.044602

I. INTRODUCTION

Taylor's hypothesis of frozen flow [1] has frequently been used to convert temporal experimental measurements into a spatial domain. Thus Taylor's hypothesis, also know as frozen turbulence hypothesis, can similarly be used to infer time dependencies from the spatial descriptions of turbulence. Its validity is of crucial importance for experimental studies and theoretical investigations.

Taylor's frozen-flow hypothesis supposes that small-scale eddies in turbulent flows move downstream with little distortion. Temporal and spatial fluctuations in turbulent flows can thus be related and, for example, temporal spectra from experimental measurements can be converted into spatial spectra. Hot-wire measurements in turbulent flows often implicitly assume its validity. Theoretically, it is also of utmost importance to understand convection in turbulent flows and the related temporal-to-spatial intermittency. Moreover, both play an important role in two-point closure turbulence models for space-time correlations in Eulerian and Lagrangian reference frames [2]. However, Taylor's hypothesis has many limitations, such as the requirements of weak shear rates and low turbulence intensities.

Discussions on its validity have a long history and are still subject to some controversy in the recent literature. For example, Del Alamo and Jiménez [3] proposed corrections to Taylor's hypothesis in turbulent boundary layers and they show "that Taylor's approximation not only

*jacobitz@sandiego.edu
†kai.schneider@univ-amu.fr

displaces the large scales near the wall to shorter apparent wavelengths but also modifies the shape of the spectrum, giving rise to spurious peaks similar to those observed in some experiments." Moin [4] points out that "clearly, experimental shear flow data based on Taylor's approximation will now need to be reconsidered."

Buchhave and Velte [5] proposed a method for converting time measurements of velocity signals into spatial information with the use of consecutive convection elements. In this approach, the local mean velocity is replaced by the instantaneous velocity magnitude, which has to be measured with its spatial flux. This increases the experimental effort, but it provides a corrected approach to get insight into spatial structure of the flow from time measurements, while avoiding the use of Taylor's hypothesis.

Motivated by the random Taylor hypothesis or sweeping decorrelation hypothesis, stating that "small eddies in turbulent flow being swept past a stationary Eulerian observer cf. [6]," acceleration fluctuations and their different contributions have been studied in Pinsky *et al.* [7] and Tsinober *et al.* [8] for isotropic turbulence. Their work is based on the prediction of Tennekes [6], which states that the Lagrangian acceleration must be small, justified by the consideration of Eulerian and Lagrangian time scales: "The hypothesis states that the velocity fluctuations at a certain point of the turbulence are caused mainly by advection, and the full (Lagrangian) accelerations of a fluid parcel turn out to be zero. In other words, the complete compensation of temporal (local) and inertial accelerations takes place [7]." The different contributions of the acceleration contributions in isotropic turbulence have been revisited recently for high-resolution direct numerical simulations [9] and a scaling of the variance with the Reynolds number has been proposed.

Homogeneous turbulent shear flow has been investigated as a prototypical example of turbulence due to the importance of shear production in the geophysical environment and in many engineering applications. In homogeneous flows, the statistical properties of turbulence do not change in the spatial directions, but they evolve in time. While this simplification has been used extensively as the basis of numerical simulations, homogeneous turbulent shear flow was first studied experimentally. Rose [10] and Champagne *et al.* [11] are credited with the first experimental studies of homogeneous turbulent shear flow. Rohr *et al.* [12] established that the eventual evolution of homogeneous turbulent shear flow follows an exponential growth law. Using direct numerical simulations, Jacobitz *et al.* [13] confirmed the exponential evolution and also investigated the impact of buoyancy forces on the flow. This prototypical flow has been studied extensively including the effects of buoyancy and rotation as well as using a variety of statistical methods e.g. [14].

Motivated by and in the continuity of our recent work in Jacobitz and Schneider [15], in which we studied the Lagrangian and Eulerian acceleration properties of fluid particles in homogeneous turbulence with uniform shear and uniform stable stratification, we generalize and extend this approach here to investigate scale dependent geometrical statistics. A wavelet-based scale-dependent decomposition of the Eulerian and convective accelerations is performed and the alignment properties are analyzed at different scales of the turbulent motion using an orthogonal wavelet decomposition e.g. [16]. The aim of this work is to address the applicability of Taylor's hypothesis at small scales in homogeneous turbulent shear flow. Lin [17] concluded: "There is, therefore, no general justification of extending Taylor's hypothesis to the case of shear flow." While this statement remains of course correct for homogeneous turbulent shear flows, Taylor's hypothesis may be applicable to a range of scales of the turbulent motion in shear flows. Tennekes [6] suggested that Taylor's hypothesis may indeed apply to the small-scale motion advected by larger scales or a mean-flow component: "In turbulence at high Reynolds numbers, therefore, the dissipative eddies flow past an Eulerian observer in a time much shorter than the time scale which characterizes their own dynamics. This suggests that Taylor's 'frozen-turbulence' approximation should be valid for the analysis of the consequences of large-scale advection of the turbulent microstructure."

The remainder of the manuscript first presents the computational background, describing the direct numerical simulations approach, the scale-dependent statistics based on an orthogonal wavelet decomposition, and the scale-dependent alignment of Eulerian and convective accelerations. Then results on the flow evolution, the alignment properties of the accelerations for the total flow and

TABLE I. Properties of the flow at $St = 4$, 7, and 10.

St	$St = 4$	$St = 7$	$St = 10$
Re_λ	103.43	136.40	156.90
SK/ϵ	4.40763	5.49498	5.22344
$\mathscr{L}$	0.83337	0.95673	0.99902
λ	0.09090	0.10149	0.09895
η	0.00598	0.00581	0.00528

at different scales of the motion, and scale-dependent geometric statistics are presented. Finally, conclusions complete the manuscript.

II. COMPUTATIONAL APPROACH

A. Simulation approach

The coordinates $\boldsymbol{x} = (x, y, z) = (x_1, x_2, x_3)$ are directed in the downstream, vertical, and spanwise directions, respectively. The downstream component of the mean velocity $\boldsymbol{U} = (U, V, W)$ has a constant gradient S in the vertical direction y:

$$U = Sy, \quad V = W = 0. \tag{1}$$

This study is based on the Navier–Stokes equations for incompressible flow. This results in the following equation of motion for the fluctuating velocity components $\boldsymbol{u} = (u, v, w) = (u_1, u_2, u_3)$ and pressure p:

$$\nabla \cdot \boldsymbol{u} = 0, \tag{2}$$

$$\frac{\partial \boldsymbol{u}}{\partial t} + \boldsymbol{u} \cdot \nabla \boldsymbol{u} + Sy\frac{\partial \boldsymbol{u}}{\partial x} + Sv\boldsymbol{e}_x = -\frac{1}{\rho_0}\nabla p + \nu\nabla^2\boldsymbol{u}. \tag{3}$$

Here, $S = \partial U/\partial y$ is the shear rate, ρ_0 the density, and ν the kinematic viscosity. The unit vector in the downstream direction is denoted as $\boldsymbol{e}_x$.

The equations of motion are transformed into a frame of reference moving with the mean velocity [18]. This transformation enables the application of periodic boundary conditions for the fluctuating components of velocity and pressure. A spectral collocation method is used for the spatial discretization and the solution is advanced in time with a fourth-order Runge-Kutta scheme. The simulations are performed in a cubic computational domain of size $L_0^3 = (2\pi)^3$ using 512^3 grid points.

The initial conditions are taken from a separate simulation of isotropic turbulence, which was allowed to develop for approximately one eddy turnover time. The initial value of the Taylor-microscale Reynolds number is $Re_\lambda = q\lambda/\nu = 89$ and $SK/\epsilon = 2$ for the shear number. Some details about the evolution of the flow are shown in Table I. The table includes the evolution of Re_λ, SK/ϵ, the integral length scale $\mathscr{L} = 2\pi \int E(k)/k dk / \int E(k) dk$, the Taylor microscale $\lambda = (10\nu K/\epsilon)^{1/2}$, and the Kolmogorov scale $\eta = (\nu^3/\epsilon)^{1/4}$. Here $q = \langle u_i u_i \rangle^{1/2}$ is the magnitude of the velocity fluctuations, $K = q^2/2$ the turbulent kinetic energy, and $\epsilon = \nu\langle \partial u_i/\partial u_k \partial u_i/\partial u_k \rangle$ its dissipation rate. The brackets $\langle \cdot \rangle$ denote a volume average at a fixed time, which is an appropriate choice for homogeneous flows.

The impact of the shear number SK/ϵ on the evolution of homogeneous turbulent shear flow has been studied in a number of previous investigations, often in the context of other parameters, such as the Reynolds number Re_λ, the Richardson number $Ri = N^2/S^2$ for stratified shear flows, or the rotation number f/S for rotating shear flows. Here, N is the Brunt-Väisälä frequency with $N^2 = -g/\rho_0 S_\rho$, where g is the gravity acceleration, ρ_0 the ambient density, and $S_\rho = \partial\rho/\partial y$ the stratification rate. The Coriolis parameter f is twice the system rotation. The first comprehensive

study of the shear number was performed by Jacobitz *et al.* [13] for homogeneous turbulent stratified shear flow, but the relevant findings also apply to the unstratified case cf. [19]. Three regimes were observed: For very low initial values of the shear number [$SK/\epsilon < O(1)$], turbulence production is too weak to sustain shear-driven turbulence and the fluctuations decay. For moderate values [$O(1) < SK/\epsilon < O(10)$], nonlinear growth of the turbulence is obtained. The simulation in this study falls into this parameter range. For large values [$SK/\epsilon > O(10)$], linear effects prevail and the evolution falls into the linear theory (or rapid distortion) limit. In the moderate regime, a final value of about five is obtained for the shear number. Shih *et al.* [20] argue that the final value of the shear number depends on the Reynolds number for small Re_λ, but that it becomes Reynolds-number independent for sufficiently large Re_λ. Linear theory has been applied to such flows by Hanazaki and Hunt [21] or Salhi *et al.* [14]. A detailed study of rotating turbulent shear flow has been performed by Brethouwer [22] at high values of the shear number. His parameter choice was motivated by the high values of SK/ϵ observed in the buffer layer close to the solid surface in wall-bounded flows (see Fig. 2 in Brethouwer [22]).

The Lagrangian and Eulerian accelerations $\boldsymbol{a}_L = \boldsymbol{a}_E + \boldsymbol{a}_C$, where $\boldsymbol{a}_C$ denotes the convective contribution, are defined as

$$\boldsymbol{a}_L = \frac{\partial \boldsymbol{u}}{\partial t} + \boldsymbol{u} \cdot \nabla \boldsymbol{u} \quad \text{and} \quad \boldsymbol{a}_E = \frac{\partial \boldsymbol{u}}{\partial t}, \tag{4}$$

respectively. The pressure-gradient term is given by $\boldsymbol{a}_P = \boldsymbol{\nabla}(p/\rho_0)$. The effect of shear is considered as an external force.

B. Scale-dependent statistics

A three-dimensional orthogonal vector-valued wavelet decomposition is used for defining scale-dependent alignment statistics of the acceleration contributions defined above. For reviews on wavelets in fluid mechanics we refer to Farge [23] as well as Schneider and Vasilyev [24]. We consider a generic vector field $\boldsymbol{a} = (a_1, a_2, a_3)$ at a fixed-time instant and decompose each component $a_\alpha(\boldsymbol{x})$ into an orthogonal wavelet series

$$a_\alpha(\boldsymbol{x}) = \sum_\lambda \widetilde{a}_\lambda^\alpha \, \psi_\lambda(\boldsymbol{x}). \tag{5}$$

The wavelet coefficients are given by the scalar product $\widetilde{a}^\alpha = \langle a_\alpha, \psi_\lambda \rangle$ e.g. [16]. The wavelets ψ_λ with the multi-index $\lambda = (j, \boldsymbol{i}, d)$ are well localized in scale $L_0 2^{-j}$ (where L_0 corresponds to the size of the computational domain), around position $L_0 \boldsymbol{i}/2^j$, and orientated in one of the seven directions $d = 1, \ldots, 7$, respectively. The three components a_α at scale $L_0 2^{-j}$ can be reconstructed by summing only over the position $\boldsymbol{i}$ and direction d indices in Eq. (5). The result yields the vector field $\boldsymbol{a}^j$ at scale $L_0 2^{-j}$. Summing all scale contributions yields the total vector field $\boldsymbol{a} = \sum_j \boldsymbol{a}^j$, as the $\boldsymbol{a}^j$ are mutually orthogonal. Table II provides values for the scale index j, the corresponding mean wave number $k_j = k_0 2^j$, and the corresponding mean physical scale $L_j = L_0 2^{-j}$. The normalized quantities in Table II, using either the Kolmogorov scale η or the Taylor microscale λ, show that the scale index values $j = 3$, 4, 5, and 6 are approximately in the inertial range, while the values 7 and 8 are in the dissipation range.

The scale-dependent statistical moments of the flow fields, including scale-dependent flatness, and scale-dependent probability distribution functions (pdfs), can thus be computed from $\boldsymbol{a}^j$ using classical statistical estimators. For instance, the qth order moment of $\boldsymbol{a}^j(\boldsymbol{x})$ can be defined by

$$M_q[\boldsymbol{a}^j] = \langle (\boldsymbol{a}^j)^q \rangle, \tag{6}$$

and since the wavelet has vanishing mean, the mean value vanishes with $\langle \boldsymbol{a}^j \rangle = 0$. The moments are thus central moments. These scale-dependent moments are directly related to the qth order structure functions [25], where the increment size is $\propto 2^{-j}$.

TABLE II. Comparison of the scale index j, the corresponding mean Fourier wave number $k_j = k_0 2^j$, and the corresponding mean physical scale $L_j = L_0 2^{-j}$ for $St = 10$. Quantities normalized either with the Kolmogorov scale η or the Taylor microscale λ are also shown.

j	k_j	L_j	$k_j\eta$	L_j/η	$k_j\lambda$	L_j/λ
0	0.77	6.28319	0.00407	1189.34	0.07619	63.49612
1	1.54	3.14159	0.00814	594.67	0.15239	31.74806
2	3.08	1.57080	0.01627	297.33	0.30478	15.87403
3	6.16	0.78540	0.03254	148.67	0.60956	7.93701
4	12.32	0.39270	0.06509	74.33	1.21911	3.96851
5	24.64	0.19635	0.13017	37.17	2.43822	1.98425
6	49.28	0.09817	0.26034	18.58	4.87645	0.99213
7	98.56	0.04909	0.52069	9.29	9.75289	0.49606
8	197.12	0.02454	1.04137	4.65	19.50578	0.24803

The scale-dependent flatness, which measures the intermittency of $\boldsymbol{a}^j$ at scale 2^{-j}, is defined by

$$Fl[\boldsymbol{a}^j] = \frac{M_4[\boldsymbol{a}^j]}{(M_2[\boldsymbol{a}^j])^2}. \tag{7}$$

For a Gaussian distribution the flatness equals three at all scales.

C. Accelerations

Tsinober *et al.* [8] considered the the alignment properties of the Eulerian acceleration $\boldsymbol{a}_E$, the convective acceleration $\boldsymbol{a}_C$, and, corresponding to its sum, the Lagrangian acceleration $\boldsymbol{a}_L = \boldsymbol{a}_E + \boldsymbol{a}_C$.

$$\langle \boldsymbol{a}_L, \boldsymbol{a}_L \rangle = \langle \boldsymbol{a}_E + \boldsymbol{a}_C, \boldsymbol{a}_E + \boldsymbol{a}_C \rangle = \langle \boldsymbol{a}_E, \boldsymbol{a}_E \rangle + \langle \boldsymbol{a}_C, \boldsymbol{a}_C \rangle + 2\cos(\boldsymbol{a}_E, \boldsymbol{a}_C)\, ||\boldsymbol{a}_E||\, ||\boldsymbol{a}_C||. \tag{8}$$

This equation allows us to statistically assess the magnitude of the Lagrangian acceleration and it also formed the starting point of our previous work in Jacobitz and Schneider [26]. In the case of an antiparallel allignment of the Eulerian acceleration $\boldsymbol{a}_E$ and the convective acceleration $\boldsymbol{a}_C$, the magnitude of the Lagrangian acceleration $\boldsymbol{a}_L$ remains small compared to those of the Eulerian and convective contributions.

Note that Eq. (8) holds not only for the total accelerations, but also for their scalewise contributions. Due to the orthogonality of the wavelet decomposition the mixed terms between different scales vanish. Hence, an application of the wavelet decomposition to the different accelerations in Eq. (5) allows us to study the scale-dependent alignment properties of the Eulerian and convective accelerations, in addition to their total fields, and check the implication for the scale-dependent Lagrangian acceleration. In the results section, we will present both the scale-dependent joint pdfs of $\boldsymbol{a}_E^j$ and $\boldsymbol{a}_C^j$ as well as the cosine of the alignment angles between the two accelerations $\cos(\boldsymbol{a}_E^j, \boldsymbol{a}_C^j)$.

From Eq. (8) we can directly conclude that, for an antialignment of Eulerian acceleration $\boldsymbol{a}_E^j$ and the convective acceleration $\boldsymbol{a}_C^j$ with a resulting negative cosine term, the norm of the Lagrangian acceleration $\boldsymbol{a}_L^j$ becomes minimal. Hence, for a perfect antialignment of $\boldsymbol{a}_E^j$ and $\boldsymbol{a}_C^j$, $\boldsymbol{a}_L^j$ would vanish, Taylor's hypothesis would hold, and temporal variations would thus correspond to the spatial variations. Hence, the departure of alignment yields a measure for how well Taylor's "approximation" holds at different scales of motion, based on the direct numerical simulation results.

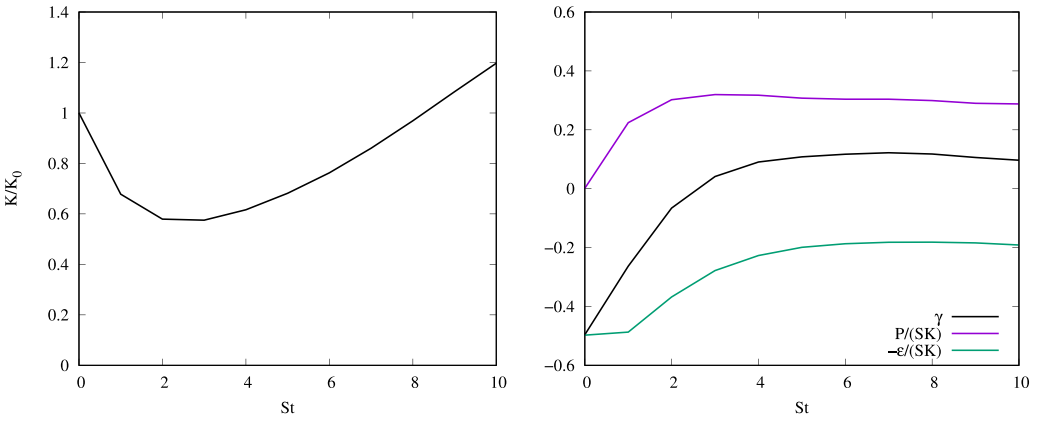

FIG. 1. Evolution of the normalized turbulent kinetic energy K/K_0 with normalized time St (left) as well as the growth rate of the turbulent kinetic energy γ, the normalized production rate $P/(SK)$, and the normalized dissipation rate $\epsilon/(SK)$ (right).

III. RESULTS AND DISCUSSION

A. Flow evolution

Figure 1 (left) provides the evolution of the turbulent kinetic energy K normalized by its initial value K_0. The turbulent kinetic energy initially decays due to the isotropic initial conditions, starts to grow at about $St = 2$, and eventually grows exponentially starting at about $St = 4$. The evolution equation for K can be written in the following nondimensional form:

$$\gamma = \frac{1}{SK}\frac{dK}{dt} = \frac{P}{SK} - \frac{\epsilon}{SK}. \tag{9}$$

Here, γ is the growth rate of the turbulent kinetic energy, $P/(SK) = -2b_{12}$ its normalized production rate, and $\epsilon/(SK)$ the normalized dissipation rate. The normalized production rate is directly related to the b_{12} component of the Reynolds stress anisotropy tensor $b_{ij} = \langle u_i u_j\rangle/\langle u_k u_k\rangle - \delta_{ij}$ and hence directly related to the anisotropy features of the flow. The evolution of γ, $P/(SK)$, and $-\epsilon/(SK)$ is shown in Fig. 1 (right) and the three terms are approximately constant for $St \geqslant 4$. Once the normalized production and dissipation rates have reached constant values, resulting in a constant growth rate γ, Eq. (9) can be integrated to obtain

$$K = Ce^{\gamma St}, \tag{10}$$

where C is a constant. In the following, the flow is analyzed in the exponential growth regime with $St \geqslant 4$ to assess the applicability of Taylor's hypothesis in homogeneous turbulent shear flow.

Figure 2 provides the joint probability distribution function (pdf) of the Eulerian acceleration $\boldsymbol{a}_E$ and the convective acceleration $\boldsymbol{a}_C$ at nondimensional time $St = 10$. Note that for $St = 4$ and 7 a very similar behavior is observed and the figures are thus omitted. The joint pdf shows an anticorrelation, which can be further quantified using the Pearson product-moment correlation coefficient r. The Pearson product-moment correlation coefficient for vector-valued quantities is defined [27] as

$$r[X, Y] = \frac{\sum_{i=1}^{M}(X_i - \overline{X})(Y_i - \overline{Y})}{\sqrt{\sum_{i=1}^{M}(X_i - \overline{X})^2 \sum_{i=1}^{M}(Y_i - \overline{Y})^2}}, \tag{11}$$

where $\overline{X}$ and $\overline{Y}$ are the mean values of the corresponding variables and $M = 512^3$ denotes the total number of grid points. The Pearson coefficient $r[\cdot, \cdot]$ ranges between -1 and 1. Values of 1 and -1

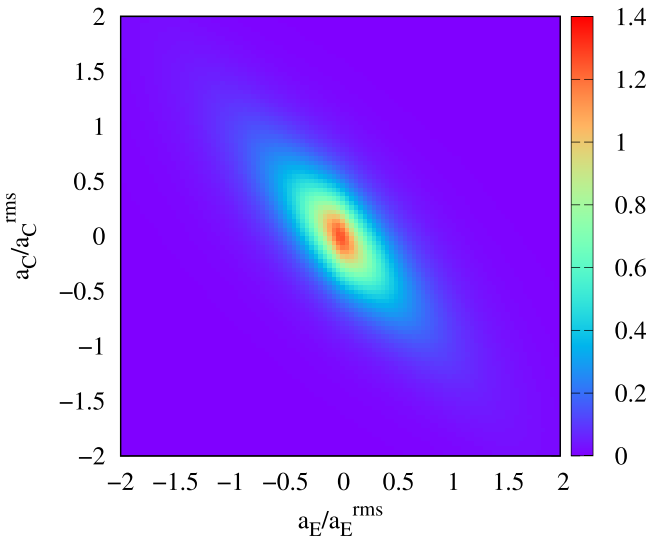

FIG. 2. Joint probability distribution functions (pdf) of the the Eulerian acceleration $\boldsymbol{a}_E$ and the convective acceleration $\boldsymbol{a}_C$ at nondimensional time $St = 10$ for the total fields.

indicate, respectively, perfect positive and negative linear correlation between the two variables. A vanishing r value signifies that there is no linear correlation between the variables.

Pearson product-moment correlation coefficient of the Eulerian acceleration $\boldsymbol{a}_E$ and the convective acceleration $\boldsymbol{a}_C$ is -0.79612. This indicates that Taylor's hypothesis cannot be applied to homogeneous turbulent shear flows in general.

B. Scale-dependent statistics

While the joint pdf for the total Eulerian acceleration $\boldsymbol{a}_E$ and the total convective acceleration $\boldsymbol{a}_C$ shows some level of anticorrelation as discussed above, a more detailed analysis is now provided for decomposed fields at different scales of the turbulent motion.

Figure 3 provides the pdfs of the Eulerian acceleration $\boldsymbol{a}_E$ and the convective acceleration $\boldsymbol{a}_C$ for the decomposed fields as a function of scale index j at nondimensional time $St = 10$. The joint pdfs clearly become more and more negatively correlated as the scale index j increases and the scale L of the motion decreases. For the large scale for $j = 2$ no strong correlation is obtained, in the inertial range ($j = 4$ and 6) the correlation becomes more pronounced, and in the dissipation ($j = 8$) strong correlation is observed.

Table III shows the Pearson correlation coefficient r between the Eulerian acceleration $\boldsymbol{a}_E$ and the convective acceleration $\boldsymbol{a}_C$ as a function of scale index j and nondimensional time St. For all times, a negative value of about $r = -0.8$ is found for the total fields. For a given time St, the value of r decreases with increasing scale index j or decreasing scale of the turbulent motion. For the smaller scales of the turbulent motion with scale index $j \geqslant 4$, the results obtained for r at different times St remain approximately the same. For the larger scales of the turbulent motion with scale indices $1 \leqslant j \leqslant 3$, the results for r decrease with time St and a stronger antialignment is observed for later times. Only the results for $j = 0$ show a different trend, but only few wavelet modes contribute to this value for r. Table III also gives the Taylor-microscale Reynolds number corresponding to the different times in the flow's evolution with later times corresponding to higher Reynolds numbers due to the exponential evolution of the flow.

Results of the second-order moments of the Eulerian, Langrangian, and convective accelerations as well as their ratios is provided in Table IV for nondimensional time $St = 10$. The second-order

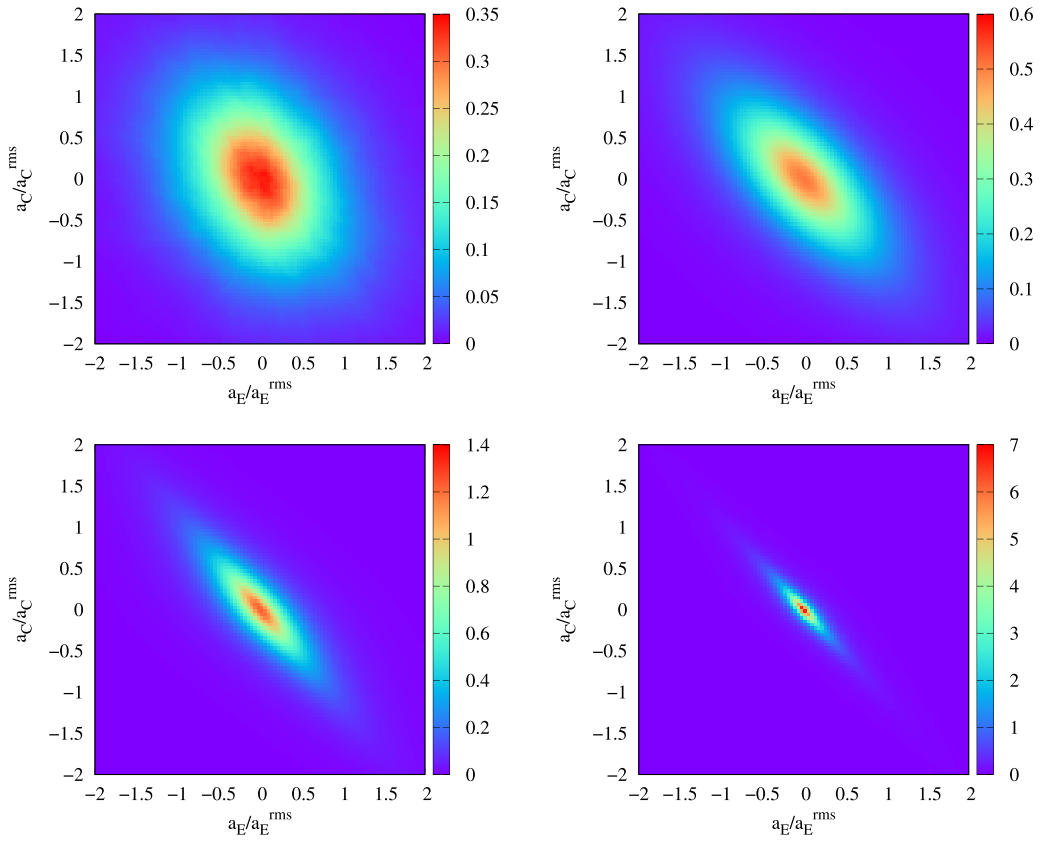

FIG. 3. Joint probability distribution functions (pdfs) of the the Eulerian acceleration $\boldsymbol{a}_E$ and the convective acceleration $\boldsymbol{a}_C$ at nondimensional time $St = 10$ for the decomposed fields at scale indices $j = 2$ (top, left), $j = 4$ (top, right), $j = 6$ (bottom, left), and $j = 8$ (bottom, right).

TABLE III. Pearson correlation coefficient between the Eulerian acceleration $\boldsymbol{a}_E$ and the convective acceleration $\boldsymbol{a}_C$ as a function of scale index j and nondimensional time $St = 4$, 7, and 10 or Taylor-microscale Reynolds number Re_λ.

St	$St = 4$	$St = 7$	$St = 10$
Re_λ	103.43	136.40	156.90
total	−0.79688	−0.79152	−0.79612
$r(j = 0)$	−0.20819	−0.48831	0.22471
$r(j = 1)$	−0.01186	−0.17431	−0.23597
$r(j = 2)$	−0.23966	−0.34748	−0.36848
$r(j = 3)$	−0.52569	−0.55758	−0.58615
$r(j = 4)$	−0.67770	−0.68890	−0.69352
$r(j = 5)$	−0.75734	−0.75537	−0.75556
$r(j = 6)$	−0.81143	−0.80741	−0.80288
$r(j = 7)$	−0.86320	−0.86073	−0.85560
$r(j = 8)$	−0.89679	−0.90279	−0.90486

TABLE IV. Scale-dependent normalized second-order moments of the acceleration $(a_E^j/a_E)^2$, $(a_L^j/a_L)^2$, and $(a_C^j/a_C)^2$ as well as ratios $(a_L^j/a_E^j)^2$ and $(a_C^j/a_E^j)^2$ at nondimensional time $St = 10$.

j	$(a_E^j/a_E)^2$	$(a_L^j/a_L)^2$	$(a_C^j/a_C)^2$	$(a_L^j/a_E^j)^2$	$(a_C^j/a_E^j)^2$
0	0.00004	0.00012	0.00001	1.82584	0.50608
1	0.00064	0.00127	0.00017	1.10789	0.41017
2	0.00289	0.00706	0.00218	1.35471	1.14237
3	0.01485	0.03253	0.01744	1.21347	1.77558
4	0.07358	0.12109	0.08483	0.91177	1.74292
5	0.22530	0.29025	0.24764	0.71373	1.66164
6	0.36185	0.35401	0.36503	0.54201	1.52498
7	0.25306	0.16645	0.22764	0.36440	1.35991
8	0.06780	0.02722	0.05505	0.22244	1.22740

moments of each acceleration at scale index j is normalized with its corresponding second-order moment of the total acceleration. All three normalized accelerations $(a_E^j/a_E)^2$, $(a_L^j/a_L)^2$, and $(a_C^j/a_C)^2$ show the same trend. Their values first increase with scale index $j \leqslant 6$ for the large-scale motion and in the inertial range. They then decrease again in the dissipation range with $j = 7$ and 8.

Their ratios, however, show different trends. The ratio of the second-order moments of Lagrangian to Eulerian acceleration $(a_L^j/a_E^j)^2$ are larger than 1 for scale indices $j \leqslant 3$. They then decrease for $j \geqslant 4$, eventually by almost an order of magnitude. This result reflects the cancellation of a_E and a_C. The ratio of the second-order moments of convective to Eulerian acceleration $(a_C^j/a_E^j)^2$, however, is smallest for the largest scales of turbulent motion at scale indices $j = 0$ and 1. In this range, the Lagrangian and Eulerian accelerations show alignment [15]. For the remaining range of turbulent scales in the inertial and dissipation ranges with $j \geqslant 2$, the ratio $(a_C^j/a_E^j)^2$ remains between 1 and 2, allowing for a cancellation of the Eulerian and convective accelerations.

Tables V and VI provide the flatness values for the Lagrangian and Eulerian accelerations, respectively. Both the values for the total accelerations and for their scale dependence are shown. The results are presented at three nondimensional times $St = 4$, 7, and 10, corresponding to three different Reynolds numbers $Re_\lambda = 103.43$, 136.40, and 156.90. Except for the flatness values at the largest scale of motion ($j = 0$), the flatness values increase with decreasing scale of motion (or increasing j). For a given scale, the flatness values of both accelerations increase with increasing

TABLE V. Scale-dependent flatness of the Lagrangian acceleration Fl_{a_L} as a function of scale index j and nondimensional time St or Taylor-microscale Reynolds number Re_λ.

St	$St = 4$	$St = 7$	$St = 10$
Re_λ	103.43	136.40	156.90
total	13.47	20.77	27.81
$Fl(j = 0)$	3.77	6.35	6.72
$Fl(j = 1)$	3.26	3.63	3.75
$Fl(j = 2)$	4.30	4.55	4.63
$Fl(j = 3)$	4.79	5.38	5.93
$Fl(j = 4)$	5.91	6.29	7.25
$Fl(j = 5)$	8.17	10.35	12.44
$Fl(j = 6)$	16.55	25.42	30.54
$Fl(j = 7)$	45.81	107.90	111.72
$Fl(j = 8)$	82.07	298.47	327.36

TABLE VI. Scale-dependent flatness of the Eulerian acceleration Fl_{a_E} as a function of scale index j and nondimensional time $St = 4$, 7 and 10 or Taylor-microscale Reynolds number Re_λ.

St	$St = 4$	$St = 7$	$St = 10$
Re_λ	103.43	136.40	156.90
total	10.10	11.96	14.41
$Fl(j = 0)$	3.71	5.51	5.22
$Fl(j = 1)$	3.54	3.47	4.09
$Fl(j = 2)$	4.35	4.36	4.72
$Fl(j = 3)$	4.70	5.43	5.53
$Fl(j = 4)$	5.86	6.01	6.55
$Fl(j = 5)$	7.30	7.70	8.22
$Fl(j = 6)$	9.69	11.35	12.45
$Fl(j = 7)$	16.63	22.57	25.92
$Fl(j = 8)$	32.88	47.88	56.43

nondimensional time St and increasing Reynolds number Re_λ. While the flatness values of the total Lagragian acceleration are always larger than those of the corresponding total Eulerian acceleration, this result does not hold at all scales of motion. For the larger scales of the motion ($0 \leqslant j \leqslant 4$), the flatness values of the two accelerations are similar. For the smaller scales of the motion ($5 \leqslant j \leqslant 8$), the flatness values of the Lagrangian acceleration are in some cases substantially larger than the corresponding values for the Eulerian acceleration.

These observations are consistent with previous work by Yoshimatsu *et al.* [28] considering homogeneous isotropic turbulence at a Reynolds number $Re_\lambda = 732$. It was observed that the flatness values of the Lagrangian and Eulerian accelerations "increase with scale [index] for the turbulent flow, but the flatness of the Lagrangian acceleration is one order of magnitude larger than the flatness of the Eulerian acceleration, which shows the extreme intermittency of the former." In a comparison to random fields with phase randomization, it was found that "the flatness remains almost constant, around 5 for the Lagrangian acceleration and around 6 for the Eulerian acceleration, which confirms that the latter yields a Laplace distribution whose flatness is 6. This proves that the random fields are non intermittent, as no scale dependence can be observed, even if their pdfs of acceleration are strongly non-Gaussian."

C. Proposed cutoff scale

A cutoff scale (in spectral space) between the scales of the turbulent motion suitable and unsuitable for an application of Taylor's hypothesis can be introduced by a consideration of the typical wave number k_S for delineating the penetration of anisotropy towards small scales [14]. For turbulent shear flows, this scale is called the Corrsin scale [29]:

$$k_S = \sqrt{\frac{S^3}{\epsilon}}. \tag{12}$$

Table VII shows the Corrsin scale as a wave number k_S, scale index j_S, and length scale L_S at times $St = 4, 7$, and 10 during the eventual evolution of the flow. As time evolves and the Reynolds number Re_λ increases, the Corrsin scale shifts to a smaller wave number, smaller scale index, and therefore larger scale of the turbulent motion. Hence, an application of Taylor's hypothesis is possible over a larger range of scales. The largest physical scales, however, remain inaccessible to an application of Taylor's hypothesis.

The Corrsin scale also delineates the regimes of flatness values observed for the Lagrangian and Eulerian accelerations reported in Tables V and VI, respectively. For the largest scales of the motion

TABLE VII. Corrsin scales expressed in wave number, as scale index, and in physical space for $St = 4, 7$, and 10.

St	$St = 4$	$St = 7$	$St = 10$
Re_λ	103.43	136.40	156.90
k_S	13.916	13.156	10.872
$k_S\eta$	0.08318	0.07646	0.05744
$k_S\lambda$	1.26498	1.33526	1.07583
j_S	4.1758	4.0947	3.8196
L_S	0.34765	0.36774	0.44500
L_S/η	58.165	63.279	84.234
L_S/λ	3.8246	3.6233	4.4971

with scale indices $j \leqslant j_S$, the flatness values of both accelerations remain relatively small, while they increase for smaller scales of the turbulent motion with scale indices $j > j_S$.

Note that the Corrsin scale k_S is part of a family of similarly-defined scales, including the Zeman scale $k_\Omega = \sqrt{f^3/\epsilon}$, where $f = 2\Omega$ is the Coriolis parameter or the Ozmidov scale $k_O = \sqrt{N^3/\epsilon}$, where $N = -g\rho_0\partial\rho/\partial y$ is the Brunt-Väisälä frequency. These two scales may help to delineate the applicability of Taylor's hypothesis in turbulent flows with rotation or stratification, respectively.

D. Scale-dependent geometric statistics

In this section, the relative orientation of vector-valued quantities is considered to strengthen the arguments made with joint pdfs above. Figure 4 shows the pdf of the cosine of the angle between different vector-valued quantities for the total and scale-dependent fields for $j = 2, 4, 6$, and 8 (from large to small scales). The following observations can be made. The Eulerian and convective accelerations have the tendency of being strongly antialigned, reflected in a peak at -1 in the pdf of $\cos(\boldsymbol{a}_E, \boldsymbol{a}_c)$ (top, left). The peak is more strongly pronounced at small scales, and weak or no alignment is found at large scales. The reason for this observation is that the advection term is essentially a small-scale quantity. This finding supports that Taylor's hypothesis holds at small scales in homogeneous turbulent shear flow. In contrast, for the pdf of $\cos(\boldsymbol{a}_L, \boldsymbol{a}_C)$ (top, right), we observe a slight probability for alignment, which becomes weaker at small scales. Consequently, the Langrangian and Eulerian accelerations are somewhat aligned (center, left), corresponding to a peak at $+1$ in the pdf of $\cos(\boldsymbol{a}_L, \boldsymbol{a}_E)$. This behavior becomes stronger for large scales. The reason is again that the convective term is a small-scale quantity and thus supports Taylor's hypothesis.

In the pdf for $\cos(\boldsymbol{a}_L, \boldsymbol{a}_p)$ we find likewise strong antialignment, which is most pronounced at intermediate scales and weakens at the largest and smallest scales (center, right). The alignment of the Lagrangian acceleration and the pressure-gradient confirms the results in Jacobitz and Schneider [15] that the pressure gradient is the dominant term contributing to the Lagrangian acceleration. The pdf of $\cos(\boldsymbol{a}_E, \boldsymbol{a}_P)$ shows some antialignment, which is stronger at large scales, and no alignment is observed at small scales (bottom, left). A similar weak antialignment behavior is found for the pdf of $\cos(a_C, a_p)$ (bottom, right).

IV. CONCLUSIONS

Direct numerical simulations of homogeneous turbulent shear flow are analyzed in order to assess Taylor's hypothesis in such flows. A scale-dependent analysis using a wavelet-based approach is performed. Taylor's hypothesis is revisited by consideration of the correlation of the Eulerian acceleration with the convective acceleration. Based on the joint pdfs and the Pearson correlation coefficients, the two accelerations show strong antialignment at small scales, indicating a cancellation of the two accelerations. However, this result does not hold for the largest scales of the

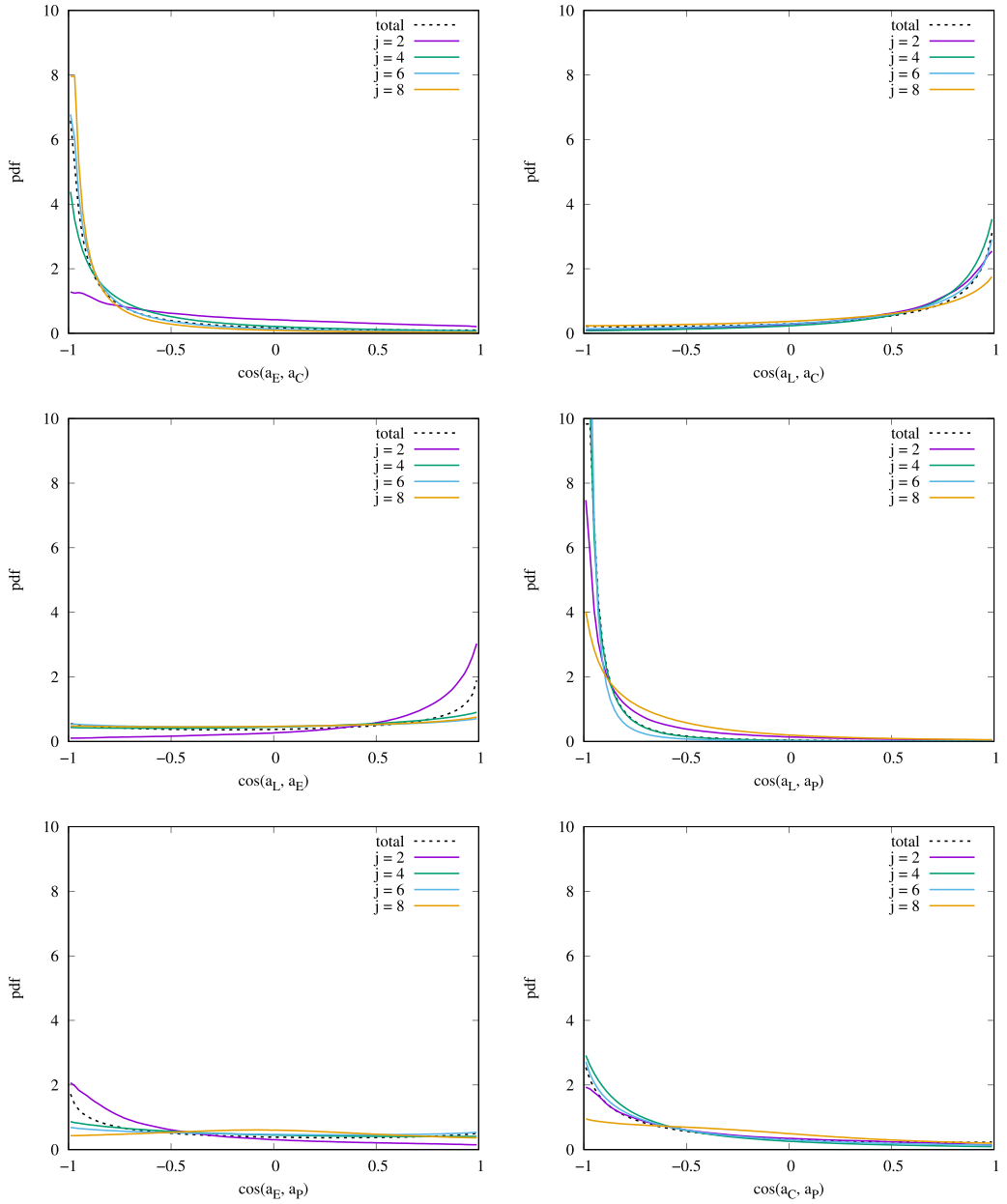

FIG. 4. Probability distribution functions (pdfs) of the cosine of the angle between the Eulerian acceleration $\boldsymbol{a}_E$ and the convective acceleration $\boldsymbol{a}_C$ (top, left), the Lagrangian acceleration $\boldsymbol{a}_L$ and the convective acceleration $\boldsymbol{a}_C$ (top, right), Lagrangian and Eulerian accelerations (center, left), Lagrangian acceleration and the pressure-gradient term (center, right), Eulerian acceleration and the pressure-gradient term (bottom, left), as well as the advection term and the pressure gradient term (bottom, right) at time $St = 10$. Note that the pdfs are shown for the total flow fields (dashed lines), and the flow fields at the scale indices $j = 2$ (large scale), 4, 6, and 8 (small scale).

motion, where only weak alignment of the two accelerations is observed. Hence, Taylor's hypothesis appears to hold at small scales in homogeneous turbulent shear flow, but not so at large scales of the motion with possible implications for instrumentalists for the turbulent kinetic energy spectra. The Corrsin scale is proposed to delineate between the two regimes. In summary, our results are in agreement with Lin [17] that there is "no general justification of extending Taylor's hypothesis to the case of shear flow." However, our results also show that, in agreement with Tennekes [6], Taylor's hypothesis is applicable to small-scale motion in homogeneous turbulent shear flow. Future work may include an expansion of the study to a larger range of shear number values and a scaling analysis with Reynolds number.

ACKNOWLEDGMENTS

K.S. acknowledges support from Agence Nationale de la Recherche, Project No. CM2E (Grant No. ANR-20-CE46-0010-01), and the French Research Federation for Fusion Studies within the framework of the Eurofusion consortium, funded by the Euratom Research and Training Programme under Grant Agreement No. 633053. F.G.J. acknowledges support from a visiting position at Aix-Marseille Université and sabbatical support from the University of San Diego. The simulations were performed on the Saber3 cluster computer at the University of San Diego. Initial results of this work were presented at the 12th Symposium on Turbulence and Shear Flow Phenomena [26].

[1] G. I. Taylor, The spectrum of turbulence, Proc. R. Soc. London, Ser. A **164**, 476 (1938).
[2] G. He, G. Jin, and Y. Yang, Space-time correlations and dynamic coupling in turbulent flows, Annu. Rev. Fluid Mech. **49**, 51 (2017).
[3] J. C. Del Alamo and J. Jiménez, Estimation of turbulent convection velocities and corrections to Taylor's approximation, J. Fluid Mech. **640**, 5 (2009).
[4] P. Moin, Revisiting Taylor's hypothesis, J. Fluid Mech. **640**, 1 (2009).
[5] P. Buchhave and C. M Velte, Measurement of turbulent spatial structure and kinetic energy spectrum by exact temporal-to-spatial mapping, Phys. Fluids **29**, 085109 (2017).
[6] H. Tennekes, Eulerian and Lagrangian time microscales in isotropic turbulence, J. Fluid Mech. **67**, 561 (1975).
[7] M. Pinsky, A. Khain, and A. Tsinober, Accelerations in isotropic and homogeneous turbulence and Taylor's hypothesis, Phys. Fluids **12**, 3195 (2000).
[8] A. Tsinober, P. Vedula, and P. K. Yeung, Random Taylor hypothesis and the behavior of local and convective accelerations in isotropic turbulence, Phys. Fluids **13**, 1974 (2001).
[9] D. Buaria and K. R. Sreenivasan, Lagrangian acceleration and its Eulerian decompositions in fully developed turbulence, Phys. Rev. Fluids **8**, L032601 (2023).
[10] W. G. Rose, Results of an attempt to generate a homogeneous turbulent shear flow, J. Fluid Mech. **25**, 97 (1966).
[11] F. H. Champagne, V. G. Harris, and S. Corrsin, Experiments on nearly homogeneous turbulent shear flow, J. Fluid Mech. **41**, 81 (1970).
[12] J. J. Rohr, E. C. Itsweire, K. N. Helland, and C. W. Van Atta, An investigation of the growth of turbulence in a uniform-mean-shear flow, J. Fluid Mech. **187**, 1 (1988).
[13] F. G. Jacobitz, S. Sarkar, and C. W. Van Atta, Direct numerical simulations of the turbulence evolution in a uniformly sheared and stably stratified flow, J. Fluid Mech. **342**, 231 (1997).
[14] A. Salhi, F. G. Jacobitz, K. Schneider, and C. Cambon, Nonlinear dynamics and anisotropic structure of rotating sheared turbulence, Phys. Rev. E **89**, 013020 (2014).
[15] F. G. Jacobitz and K. Schneider, Lagrangian and Eulerian accelerations in turbulent stratified shear flows, Phys. Rev. Fluids **6**, 074609 (2021).

[16] M. Farge and K. Schneider, Wavelet transforms and their applications to MHD and plasma turbulence: A review, J. Plasma Phys. **81**, 435810602 (2015).
[17] C. C. Lin, On Taylor's hypothesis and the acceleration terms in the Navier-Stokes equation, Q. Appl. Math. **10**, 295 (1953).
[18] R. S. Rogallo, *Numerical Experiments in Homogeneous Turbulence*, Technical Report TM 81315 (NASA Ames Research Center, Moffett Field, CA, 1981)
[19] J. C. Isaza and L. R. Collins, On the asymptotic behaviour of large-scale turbulence in homogeneous shear flow, J. Fluid Mech. **637**, 213 (2009).
[20] L. H. Shih, J. R. Koseff, J. H. Ferziger, and C. R. Rehmann, Scaling and parameterization of stratified homogeneous turbulent shear flow, J. Fluid Mech. **412**, 1 (2000).
[21] H. Hanazaki and J. C. R. Hunt, Structure of unsteady stably stratified turbulence with mean shear, J. Fluid Mech. **507**, 1 (2004).
[22] G. Brethouwer, The effect of rotation on rapidly sheared homogeneous turbulence and passive scalar transport. linear theory and direct numerical simulation, J. Fluid Mech. **542**, 305 (2005).
[23] M. Farge, Wavelet transforms and their applications to turbulence, Annu. Rev. Fluid Mech. **24**, 395 (1992).
[24] K. Schneider and O. V. Vasilyev, Wavelet methods in computational fluid dynamics, Annu. Rev. Fluid Mech. **42**, 473 (2010).
[25] K. Schneider, M. Farge, and N. Kevlahan, Spatial intermittency in two–dimensional turbulence: A wavelet approach, in *Woods Hole Mathematics, Perspectives in Mathematics and Physics* (World Scientific, Singapore, 2004), pp. 302–328.
[26] F. G. Jacobitz and K. Schneider, Scale-dependent geometric statistics of the Lagrangian and Eulerian accelerations in homogeneous turbulent shear flow, in *Proceedings of the 12th International Symposium on Turbulence and Shear Flow Phenomena (TSFP12)* (TU Darmstadt, Darmstadt, Germany, 2022).
[27] J. Lee Rodgers and W. A. Nicewander, Thirteen ways to look at the correlation coefficient, Am. Stat. **42**, 59 (1988).
[28] K. Yoshimatsu, N. Okamoto, K. Schneider, Y. Kaneda, and M. Farge, Intermittency and scale-dependent statistics in fully developed turbulence, Phys. Rev. E **79**, 026303 (2009).
[29] S. Corrsin, *Local Isotropy in Turbulent Shear Flow* (NACA, Washington, DC, 1958), Vol. 34.